Impacts of tiled land cover characterization in the Model for Prediction Across Scales-Atmosphere (MPAS-A)

Patrick Campbell[1], Jesse Owen Bash[2], Jerold A. Herwehe[2], Robert Chad Gilliam[3], and Dan Li[4]

[1]George Mason University
[2]U.S. EPA
[3]US EPA
[4]Boston University

November 24, 2022

Abstract

Parameterization of subgrid-scale variability of land cover characterization (LCC) is an active area of research, and can improve model performance compared to the dominant (i.e., most abundant tile) approach. The "Noah" land surface model implementation in the global Model for Predictions Across Scales-Atmosphere (MPAS-A), however, only uses the dominant LCC approach that leads to oversimplification in regions of highly heterogeneous LCC (e.g., urban/suburban settings). Thus, in this work we implement a subgrid tiled approach as an option in MPAS-A, version 6.0, and assess the impacts of tiled LCC on meteorological predictions for two gradually refining meshes (92-25 and 46-12 km) focused on the conterminous U.S for January and July 2016. Compared to the dominant approach, results show that using the tiled LCC leads to pronounced global changes in 2-m temperature (July global average change ~ -0.4 K), 2-m moisture, and 10-m wind speed for the 92-25 km mesh. The tiled LCC reduces mean biases in 2-m temperature (July U.S. average bias reduction ~ factor of 4) and specific humidity in the central and western U.S. for the 92-25 km mesh, improves the agreement of vertical profiles (e.g., temperature, humidity, and wind speed) with observed radiosondes, and there is a general decrease in error for precipitation in the U.S.; however, there is increased bias and error for incoming solar radiation at the surface. The inclusion of subgrid LCC has implications for reducing systematic warm biases found in numerical weather prediction models.

Impacts of tiled land cover characterization in the Model for Prediction Across Scales-Atmosphere (MPAS-A)

Patrick C. Campbell[1,2,3], Jesse O. Bash[4], Jerold A. Herwehe[4], Robert C. Gilliam[4], Dan Li[5]

[1]National Academies/National Research Council (NRC) Fellowship Participant at National Exposure Research Laboratory, U.S. Environmental Protection Agency

Research Triangle Park, North Carolina, USA

[2]Now at Center for Spatial Information Science and Systems/Cooperative Institute for Satellite Earth System Studies, George Mason University

[3]ARL/NOAA Affiliate

[4]Center for Environmental Measurement and Modeling , U.S. Environmental Protection Agency

Research Triangle Park, North Carolina, USA

[5]Department of Earth and Environment, Boston University, Boston, MA, USA

Corresponding Author: Patrick C. Campbell (patrick.c.campbell@noaa.gov)

Key Points

- The use of tiled land cover characterization (LCC) has significant impacts on global meteorological predictions in MPAS-A.
- Tiled LCC reduces bias and error for near-surface temperature, moisture, and wind speed over the U.S.
- The tiled LCC approach can help mitigate systematic warm biases in weather and climate models.

Abstract

Parameterization of subgrid-scale variability of land cover characterization (LCC) is an active area of research, and can improve model performance compared to the dominant (i.e., most abundant tile) approach. The "Noah" land surface model implementation in the global Model for Predictions Across Scales-Atmosphere (MPAS-A), however, only uses the dominant LCC approach that leads to oversimplification in regions of highly heterogeneous LCC (e.g., urban/suburban settings). Thus, in this work we implement a subgrid tiled approach as an option in MPAS-A, version 6.0, and assess the impacts of tiled LCC on meteorological predictions for two gradually refining meshes (92-25 and 46-12 km) focused on the conterminous U.S for January and July 2016. Compared to the dominant approach, results show that using the tiled LCC leads to pronounced global changes in 2-m temperature (July global average change ~ -0.4 K), 2-m moisture, and 10-m wind speed for the 92-25 km mesh. The tiled LCC reduces mean biases in 2-m temperature (July U.S. average bias reduction ~ factor of 4) and specific humidity in the central and western U.S. for the 92-25 km mesh, improves the agreement of vertical profiles (e.g., temperature, humidity, and wind speed) with observed radiosondes, and there is a general decrease in error for precipitation in the U.S.; however, there is increased bias and error for incoming solar radiation at the surface. The inclusion of subgrid LCC has implications for reducing systematic warm biases found in numerical weather prediction models.

1. Introduction

The land cover characterization (LCC), i.e., the physical characteristics of Earth's land surface (vegetated, wetlands, water, ice, or urban/impervious), is inherently heterogeneous, in some areas extreme, and is rapidly changing due to recent and projected future fluctuations in the LCC for both developed and developing countries. Changes in LCC due to human activities (e.g., deforestation, industrialization, agriculture, urban sprawl) produce physical changes in land surface albedo, latent (LH) and sensible heat (SH) fluxes, and atmospheric aerosol and greenhouse gas concentrations. Consequently, LCC changes have accounted for approximately half of the human-caused global radiative forcing from 1850 to the present day (Hibbard et al., 2017).

Numerical atmospheric, or weather prediction models (NWPs) are used to predict the near- and long-term weather and climate changes, which are tightly bound to the land surface model (LSM) component that represents the lower physical boundary, controls the representation of LCC variability, is the memory of climatic changes, and apportions the physical responses in surface LH and SH fluxes. NWP models, however, consistently simulate warmer surface temperatures compared to ground observations, where most of the systematic 2-meter temperature biases appear by day-5 predictions, and the largest warm bias is found in the Central U.S. (Ma et al., 2014). A joint model-observation intercomparison project, the Clouds Above the United States and Errors at the Surface (CAUSES), evaluated the role of clouds, radiation, and precipitation processes in contribution to the surface temperature biases in the Central U.S (Morcrette et al., 2018). One of the important findings from the CAUSES project was that the large warm bias in NWP models are attributed to the simulation of deep convective clouds and the evaporative fraction (EF = LH/[LH+SH]) at the surface (Steiner et al., 2018; and references contained within). Thus, there exists a direct connection between the accuracy of the NWP models' representation of the LCC and subgrid scale variability in its coupled LSM, and the predictive accuracy of EF and associated feedbacks with surface temperature and moisture, clouds, and precipitation.

Using a "dominant" approach to LCC in LSMs, where each grid cell is assumed to be entirely composed of the most abundant land use (LU) type, is an oversimplification of the real-world LCC variability, especially in regions with high spatial heterogeneity. Of course, in practice there must exist a balance between representing the myriad of processes that relatively coarse models cannot resolve, and the available computational efficiency and resources for the respective application of the model. Spatial variability in LCC and the resulting hydrologic and atmospheric responses, are driven by a number of factors with both random and nonrandom components. Thus, depiction of subgrid-scale LCC variability in LSMs has been an active area of research over the past three decades (Giorgi and Avissar, 1997), where Avissar and Pielke (1989) first proposed a subgrid LCC parameterization that used a number of patches (or tiles), i.e., the "tiled" approach, and showed that it resulted in strong contrasts in total surface energy fluxes. In the tiled approach, the corresponding surface fluxes, energy, and water balances in the LSM are calculated for each explicit LU category with unique vegetation attributes in the model grid cell, and then are spatially averaged to produce the surface fluxes for each cell.

Other subgrid LCC methods include the "composite" approach, which is similar to the dominant approach, but the surface properties are either linearly or non-linearly aggregated based on the properties of all the tiles within the grid cell (Koster and Suarez, 1992; Verseghy et al., 1993). The statistical-dynamical approach assumes that the land surface parameters that are critical for calculating surface fluxes follow certain probability density functions (PDFs) (Avissar, 1991; Entekhabi and Eagleson, 1989; Famiglietti and Wood, 1991). The multivariate mosaic subgrid approach (i.e., “k-means clustering”) method is used to take an arbitrary number of input descriptors and objectively determine areas of similarity within a grid cell. This is in contrast to a “univariate approach” that only uses one spatially varying parameter to aggregate a catchment into a relatively few classes (Newman et al., 2014). The k-means clustering method may in fact be well suited to represent subgrid spatial complexity in LSM applications on the global to regional scales. Other global- to regional-scale LSMs have incorporated subgrid LCC, such as the Community Land Model (CLM) that has a nested subgrid hierarchy in which grid cells are composed of multiple land units (vegetated, lake, urban, glacier, and crop), snow/soil columns, and plant functional types (PFTs). In essence this may be considered a “semi-tile” method, as each subgrid level has a physical data structure that handles quantities that are not involved in conservation checks. A true tiled scheme called “newsnow” is also an option in the European High Resolution Limited Area Model (HIRLAM), and it includes seven individual subgrid tiles that are treated with unique values of vegetation, roughness length, and albedo (Samuelsson et al., 2006; Gollvik and Samuelsson, 2011).

The unified National Center for Atmospheric Research (NCAR), Oregon State University, the U.S. Air Force, and National Centers for Environmental Prediction’s (NCEP’s) Office of Hydrology (“Noah”) LSM (Chen & Dudhia, 2001; Chen et al., 1996, 1997, 2007; Ek et al., 2003; Li et al., 2013; Mitchell et al., 2004; Niu et al., 2011; Pan & Mahrt, 1987; Yin et al.,2015) has been widely developed, applied, and evaluated in its parent atmospheric grid model, the Weather Research and Forecasting (WRF) model (Powers et al., 2017; Skamarock & Klemp, 2008). The Li et al. (2013) method of explicit tiling (referred to as the "mosaic" method) in WRF/Noah is intriguing as it maintains tile-specific surface energy flux calculations that are then weighted averages for the entire grid cell used in conservation checks. Furthermore, Li et al. demonstrated that the tiled LCC method demonstrates stark differences, better model performance, and less sensitivity to spatial grid resolution for surface energy fluxes, land surface temperature, near-surface states, boundary layer growth, as well as rainfall distribution compared against the dominant approach in Noah. However, the applications of tiled LCC in global LSMs are limited to simulated energy and carbon balances at select boreal, temperate and tropical locations across the world (Li and Arora, 2012), and do not truly investigate the global, coupled atmospheric feedbacks as a result of the tiling (Melton and Arora , 2014). Furthermore, studies that do investigate such atmospheric feedbacks to subgrid LCC are specific to regional-scale applications (Li and Arora, 2012; Li et al., 2013; Li et al., 2017; Mallard et al., 2018). We note that all the above referenced studies show that the surface parameters and energy fluxes are very sensitive to using a tiled LCC compared to a dominant or composite approach. Thus, there is a need to implement and test the impacts of tiled LCC from the global to mesoscale to assess the impacts of more realistic LU on surface energy fluxes and the feedbacks to the cloud and radiative model predictions. The effects of tiled LCC have implications for both the scientific and operational weather forecasting communities, especially in areas of highly contrasting LU types (Manrique-Suñén et al., 2013).

The atmospheric component of the Model for Predictions Across Scales-Atmosphere (MPAS-A) uses an unstructured centroidal Voronoi, nominally hexagonal mesh (grid, or tessellation) and C-grid staggering of the state variables as the basis for the horizontal discretization in the dynamical solver (Skamarock et al., 2012 and references contained within). The MPAS-A is ideal for this work as it is a parent, global atmospheric model to the Noah LSM, and the unstructured variable resolution meshes can be generated having smoothly-varying mesh transitions. The Noah implementation in MPAS-A (hereafter referred to as MPAS/Noah), however, only uses the dominant LCC approach. This results in an oversimplification in regions of highly heterogeneous LCC (e.g., urban/suburban settings), which is also impacted by the gradually refining meshes in MPAS for global to mesoscale applications. Thus, in this work we implement the tiled LCC approach as an option in MPAS/Noah, version 6.0, and assess the global-to-mesoscale impacts of tiled LCC in MPAS/Noah on meteorological predictions for two gradually refining meshes (92-25 and 46-12 km) focused on the conterminous U.S for January and July 2016. The year 2016 was chosen as relatively fine scale initial conditions are available for that year (see Section 2.2), and the January/July months represent climatological cool/warm seasons for both the Northern and Southern Hemispheres.

2. Methods

2.1 A tiled approach to LCC in MPAS-A

In this work we implement a tiled LCC to MPAS/Noah, which is analogous to the tiled (i.e., “mosaic”) approach found in the WRF model described by Li et al. (2013) (hereafter referred to as the “L13-tiled”, or simply the “tiled” approach). Generally applying the L13 approach here, a certain user-defined number (N) of tiles, each representing a land cover category, is considered within a mesh cell. The atmospheric properties and soil properties are assumed to be homogenous over the mesh cell when surface fluxes and surface state variables are calculated for each tile, and all prognostic variables are maintained for each tile, some of which are aggregated to yield the mesh cell average variables (Li et al., 2013). In the L13-tiled approach the mesh cell average variables are weighted by the normalized area fraction accounting for the areas of each tile, where the tile with the largest normalized area fraction has a rank of 1. The smaller normalized area fractions for each land cover category are subsequently given lower rankings, and the total N tiles are assumed constant for all mesh cells. This is in contrast to the dominant LCC approach, which only considers the most dominant tile (i.e., tile rank = 1), and does not consider fractional impacts of subgrid, tiled heterogeneity in LCC (Figure 1). The reader is referred to Li et al. (2013) and the references contained within for further details regarding the L13-tiled approach.

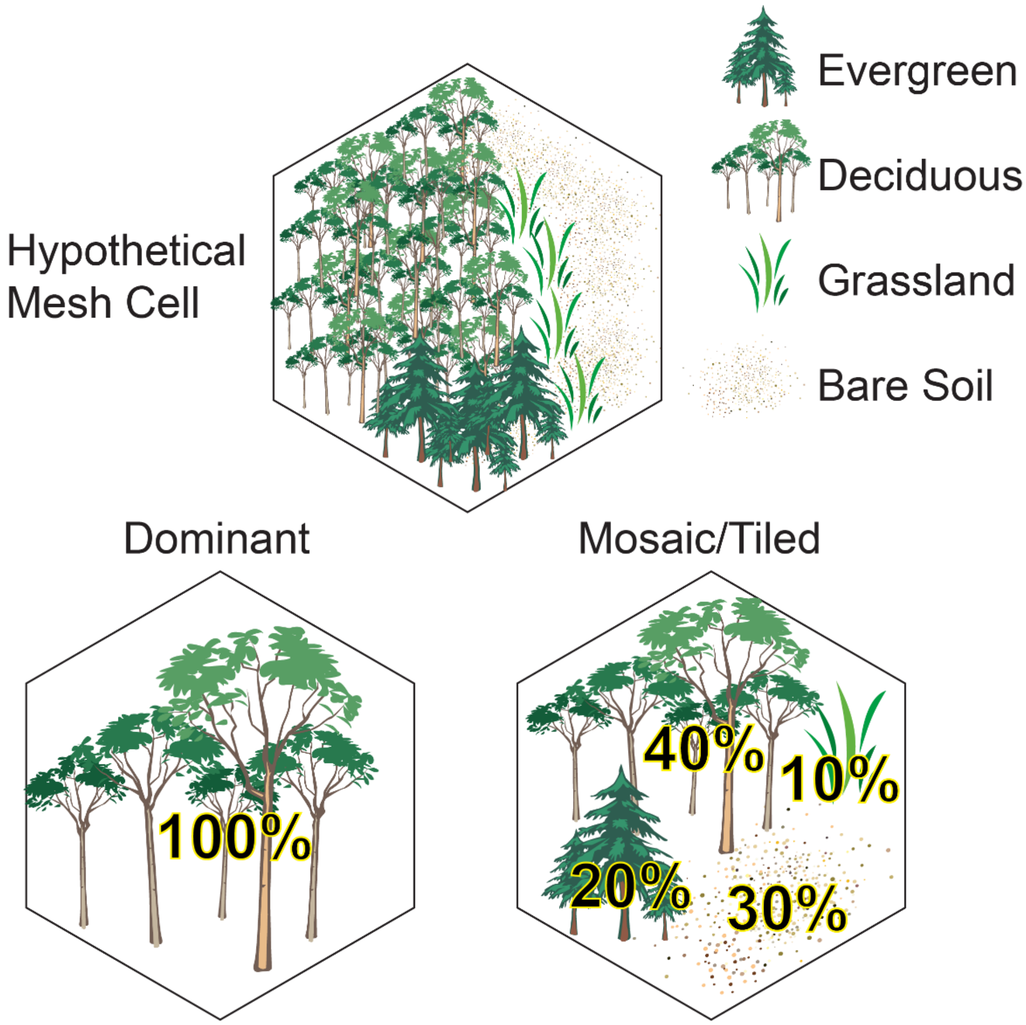

Figure 1. Illustration of a hypothetical "real-world" land cover in a hexagonal mesh cell in MPAS-A, and the corresponding dominant vs. L13-tiled approach to LCC used in the MPAS/Noah LSM.

2.2 Model configuration and simulation design

Here we apply two MPAS-A version 6.0 global meshes that seamlessly refine from a relatively coarse to fine, 92-25 and 46-12 km, horizontal grid spacing over the conterminous U.S. (CONUS). The global domain and subset of the CONUS are shown for the 92-25 km mesh in Figure 2, which also include the corresponding average vegetation fractions for January and July 2016.

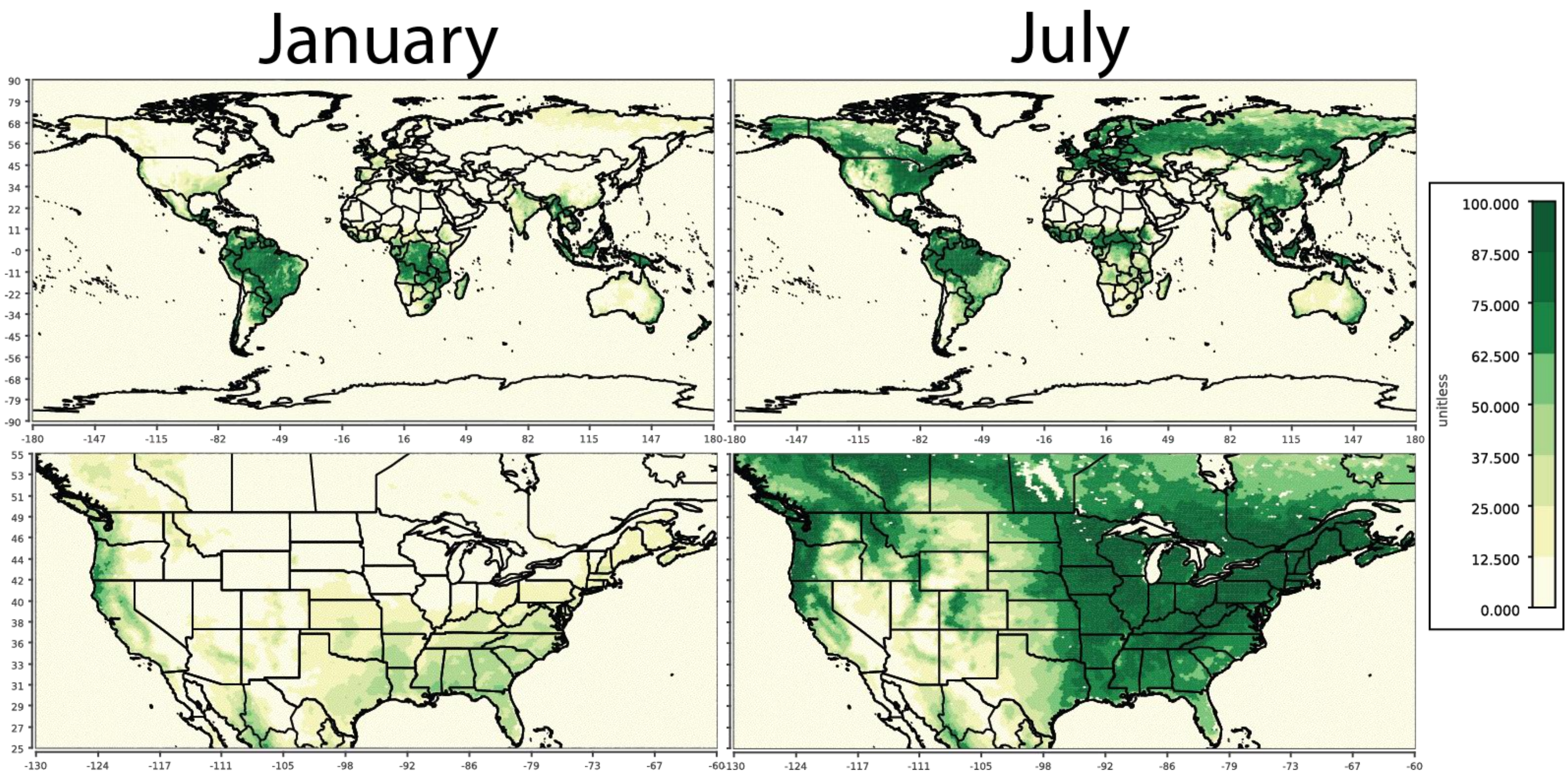

Figure 2. Global 92-25 km and seamlessly refined 25 km mesh over CONUS. The average vegetation fraction at 92-25 km is also shown for January and July 2016 .

Here we employ the default MPAS-A v6.0 default physics suite (based on the Advanced Research WRF model), except for the new implementation of the L13-tiled approach as an option to dominant LCC (default) in MPAS/Noah (Table 1). The physics options used here are a very common configuration in WRF, and thus are well documented on the WRF User's Page and references contained within (http://www2.mmm.ucar.edu/wrf/users/).

Table 1. *MPAS-A v6.0 Model Configuration*

Model Mesh/Process	**Configuration**
Mesh Resolutions with Seamless Refinement	92-25 km and 46-12 km
Time Steps	100 s (92-25 km); 40 s (46-12 km)
Land Surface Model	Dominant and *L13-tiled Noah* (N=15 tiles per cell)
Land use Data	Combined 40-Category NLCD (conterminous U.S.) and IGBP-MODIS (Global)
Surface Layer	Monin-Obukhov (MO)
Planetary Boundary Layer	Yonsei University (YSU)
Grid Microphysics/Subgrid Convection	WRF Single Moment 6-class (WSM6)/Kain-Fritsch (KF)
Radiation	Rapid Radiative Transfer Model for GCMs (RRTMG)

The meteorological initial conditions are based on NCEP operational Global Forecast System analysis and forecast grids on a 0.25° x 0.25° global latitude longitude grid (https://rda.ucar.edu/datasets/ds083.3/). A combined 40-category LU dataset is used to represent the LCC, where the National Land Cover Database (NLCD) is used within the CONUS, and elsewhere the International Geosphere-Biosphere Programme (IGBP)-Modified Moderate

Resolution Imaging Spectroradiometer (MODIS) satellite database. Independent tests of a similar WRF model configuration/domain over the U.S. also indicates that setting the number of LU tiles (N) = 8 results in about 97% of all model grid cells having 99% of their LU categories represented (Campbell et al., 2019). To ensure all MPAS/Noah mesh cells have ≥ 99% of their LU categories represented, here we employ a very conservative value of N = 15.

The simulation design consists of 1-month simulations using dominant and tiled LCC for January and July 2016, both at 92-25 and 46-12 km variable mesh grid spacing (total of 8 simulations). Each simulation applies a 10-day spin-up (not used in analysis) and 5-day reinitialization strategy (Table 2), which both reduces the error ingested from the initial conditions and helps avoid model divergence typical of longer simulation periods (e.g., multiple weeks or months).

Table 2. *MPAS-A v6.0 Model Simulation Design*

Run	MPAS/Noah LCC	Period	Mesh Resolution
#1	Dominant	January 2016	92-25 km
#2	Dominant	July 2016	92-25 km
#3	L13-tiled	January 2016	92-25 km
#4	L13-tiled	July 2016	92-25 km
#5	Dominant	January 2016	46-12 km
#6	Dominant	July 2016	46-12 km
#7	L13-tiled	January 2016	46-12 km
#8	L13-tiled	July 2016	46-12 km

The simulation design in Table 2 allows for the analysis of the impacts of L13-tiled compared to dominant LCC during both a winter and summer month, while also providing insight into the impact of the L13-tiled approach on reduction of the sensitivity of the MPAS/Noah model to different mesh resolutions.

2.3 Observations and Evaluation Protocol

Observations from both surface and upper-air platforms are used for the evaluation of MPAS-A dominant versus the tiled method and the sensitivity to the refining mesh resolution. The near-surface observations of 2-meter temperature (T2), 2-meter specific humidity (Q2), and 10-meter wind speed (WSPD10) are based on the Surface Weather Observations and Reports for Aviation Routine Weather Reports (METAR) which are collected by NCEP's Meteorological Assimilation Data Ingest System (MADIS) (https://madis.ncep.noaa.gov/madis_metar.shtml).

The shortwave radiation at the ground (SWDOWN) observations are obtained from the World Radiation Monitoring Center's (WRMC) Baseline Solar Radiation Network (BSRN) (https://bsrn.awi.de/; Driemel et al., 2018;). The precipitation observations are obtained from the Climate Group at Oregon State University's Parameter-elevation Regressions on Independent Slopes Model (PRISM) (http://www.prism.oregonstate.edu/). Vertical profile observations of temperature, relative humidity, and wind speed are obtained from the National Oceanic and Atmospheric Administration (NOAA), Earth System Research Laboratory's (ESRL) Radiosonde Database (RAOB) (https://ruc.noaa.gov/raobs/).

Typical meteorological statistical metrics are used to evaluate the performance of MPAS-A dominant versus the tiled approach, which include the mean bias (MB), root mean square error (RMSE), Pearson's correlation coefficient (R), and index of agreement (IOA). Such statistical metrics have been well defined in the available literature (e.g., Table 3 in Emery et al., 2016).

3. Results

3.1 Impacts of the tiled approach for the MPAS-A 92-25 km mesh

Globally, the tiled method's top ranked tiles (i.e., ranking of LU types by dominance) show a high heterogeneity in LU categories and associated LU fractions compared to the dominant category (Figure 3a-f). In the western U.S., the tiled method allows for forest LU fractions in cells dominated by grasses/shrubs, while in the eastern U.S., there are urban and grass/shrub fractions in cells dominated by forest LU (Figure 3g-l). Ultimately, the amount of tiled LCC heterogeneity depends on the combination of the specific input LU dataset and model cell resolution, which in this case varies from the global (IGBP-MODIS and 92 km) to the U.S. scale (NLCD and 25 km).

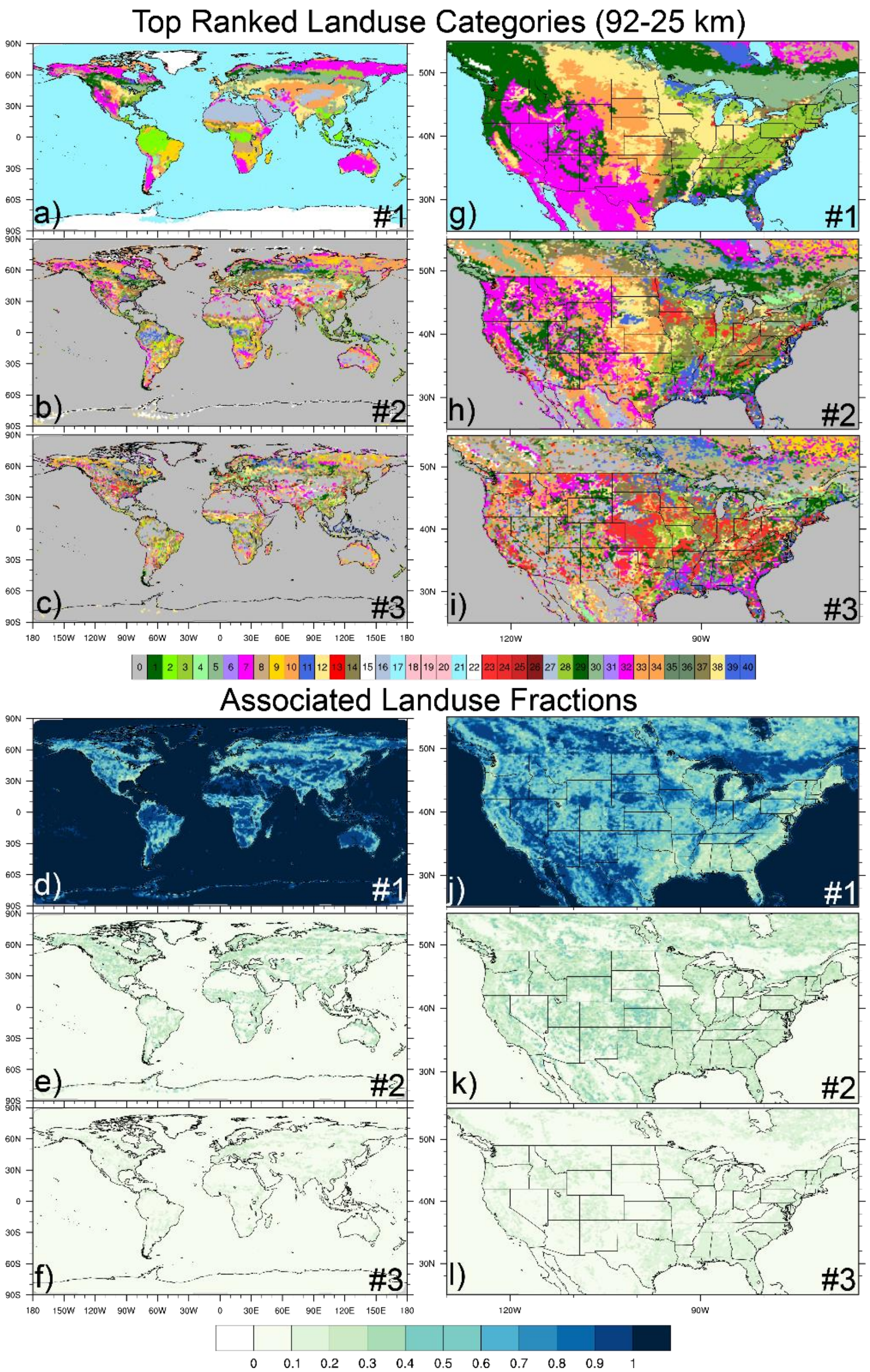

Figure 3. Spatial plots of the top three ranked (#1 = dominant LU, #2 and #3), tiled LU categories and their associated LU fractions for the combined 40-category NLCD (CONUS) and (IGBP)-Modified MODIS satellite database (elsewhere global). The IGPB-MODIS (1-17) and NLCD (21 – 40) LU categories are (combined for simplification): Forests: 1-5 & 28-30; Grasses, Shrubs, or Savannahs: 6-10 & 31-34 & 37; Lichens/Moss: 35-36; Wetlands: 11 & 39-40; Croplands: 12, 14, & 38; Urban/Developed: 13 & 23-26; Snow and Ice: 15 & 22; Barren/Sparsely Vegetated: 16 & 27; Water: 17 & 21; Unclassified: 18-20; Regions of LU fraction <0.01: 0 (Filled-grey).

Including additional LU categories in the tiled method results in global differences for the top three ranked tiled (i.e., tile #2 - #1 and #3 - #1) surface/skin temperature (TSK_{tile}), surface specific humidity ($QSFC_{tile}$), sensible heat flux (SH_flx_{tile}), latent heat flux (LH_flx_{tile}), ground heat flux (G_{tile}), and aerodynamic roughness length (Z_{tile}) in January (Figure 4) and July 2016 (Figure 5) for the 92-25 km mesh (Supporting Figure S1 also shows the albedo, ALB_{tile}, and emissivity, $EMIS_{tile}$ differences). Clearly the regions of appreciable LU fractions for tile rankings #2 and #3 (Figure 3) spatially agree well with the areas of largest changes in surface variables and fluxes, where the magnitude of TSK change is generally larger in July (e.g., Figure 4a; global avg. $\Delta TSK_{tile\#2-\#1}$ = -0.13 K) compared to January (e.g., Figure 5a; global avg. $\Delta TSK_{tile\#2-\#1}$ = -0.04 K), especially in the CONUS region application of the NLCD at the refined mesh scale (~25 km).

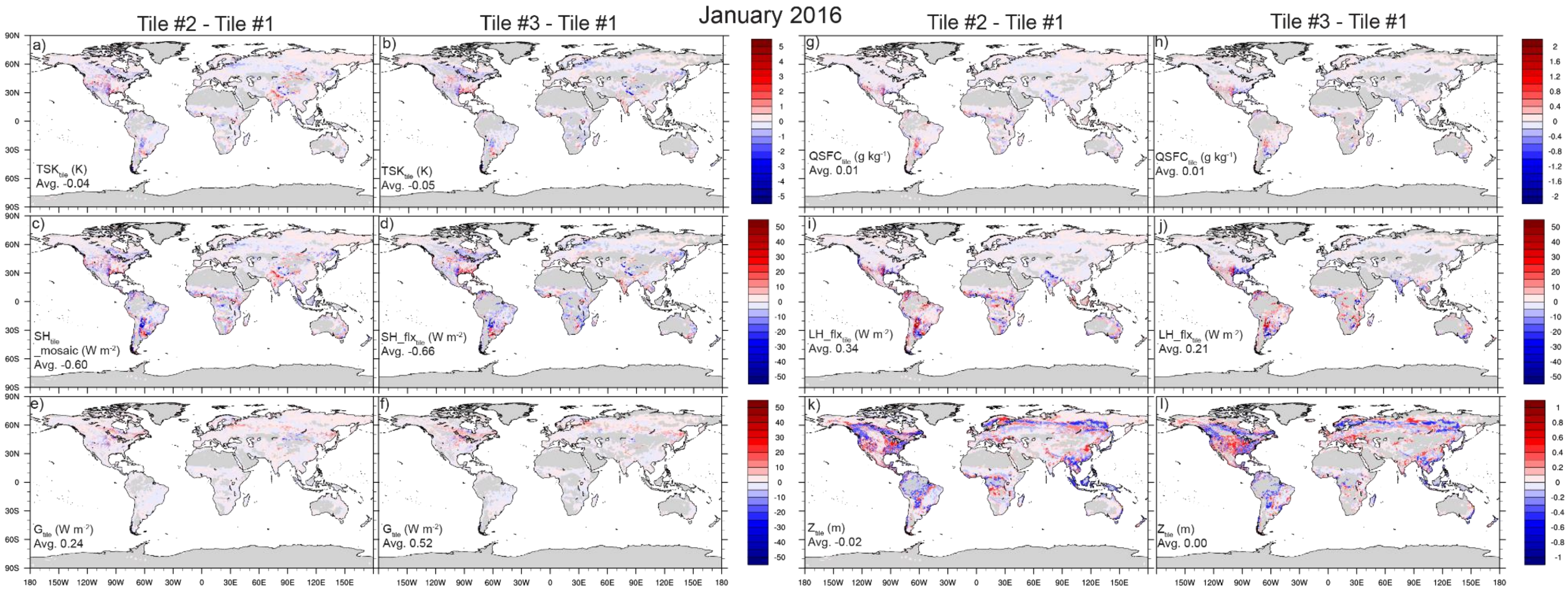

Figure 4. January 2016 average differences in the top ranked tiled LU categories (#2-#1 and #3-#1) for a)-b) TSK_{tile} , c)-d) SH_{tile}, e)-f) G_{tile}, g)-h) $QSFC_{tile}$, i)-j) LH_{tile}, and k)-l) Z_{tile} on the 92-25 km resolution mesh.

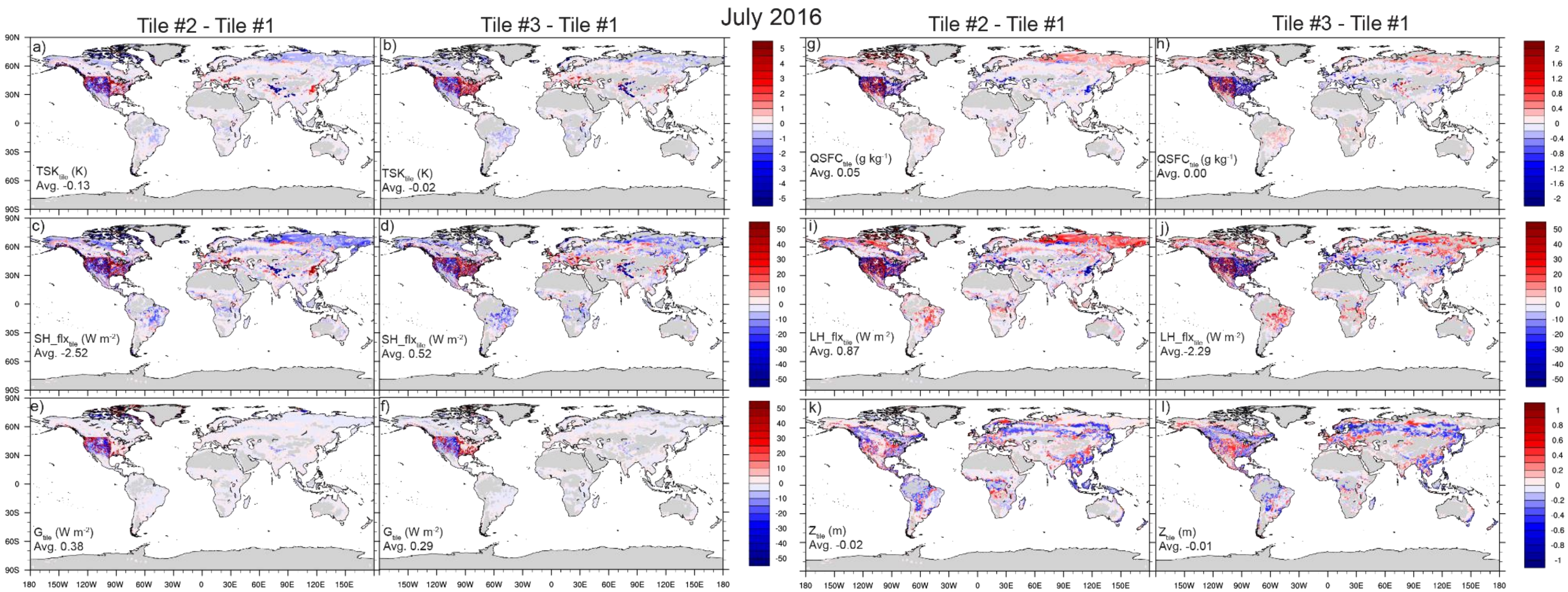

Figure 5. Same as in Figure 4, but for July 2016**.**

On average, comparing the #2 and #3 ranked tiles to the dominant (#1 rank) leads to decreased global TSK_{tile} and SH_flx_{tile}, and slightly increased G (more heat flux into the ground) in both January and July (Figures 4a-f and 5a-f). There are exceptions, however, where the #2 and #3 ranked LU tiles demonstrates increased TSK_{tile}, SH_flx_{tile}, and G_{tile}, especially in the eastern CONUS for Tile #2-1 and #3-1 in July. These increases are due to the effects that urban and crop/grasslands in the #2 and #3 ranked LU tiles have on the surface energy balance compared to the dominant deciduous and evergreen forest in mesh cells found in this region (Figure 3). In the western U.S. in July, the #2 and #3 ranked LU tiles have appreciable fractions of forests compared to the dominant grasses, shrubs, or savannahs in this region that leads to a strong cooling effect with widespread decreases in TSK_{tile}, SH_flx_{tile}, and G_{tile}.

The tiled method also impacts the aerodynamic roughness length (Z_{tile}), which have the same changes for January and July 2016 because Z_{tile} is solely a function of the tabulated LU category in the Noah LSM. On average, there is a slight decrease in Z_{tile} globally; however, there are locally larger increases and decreases dependent on the level of contrast in roughness lengths for different LU categories. For example, there are relatively large decreases in Z_{tile} in the eastern U.S. due to smaller average roughness lengths for croplands (~0.1; #2 and #3 ranked tiles) compared to the dominant forests (~0.5). Changes in roughness lengths, Z_{tile}, will have impacts on the diagnosed average wind speeds above the surface, as discussed further below.

There are prominent changes in the average January and July 2016 difference plots (tiled – dominant) for MPAS-A diagnostic variables T2, Q2, and WSPD10 at the 92-25 km resolution mesh (Figure 6).

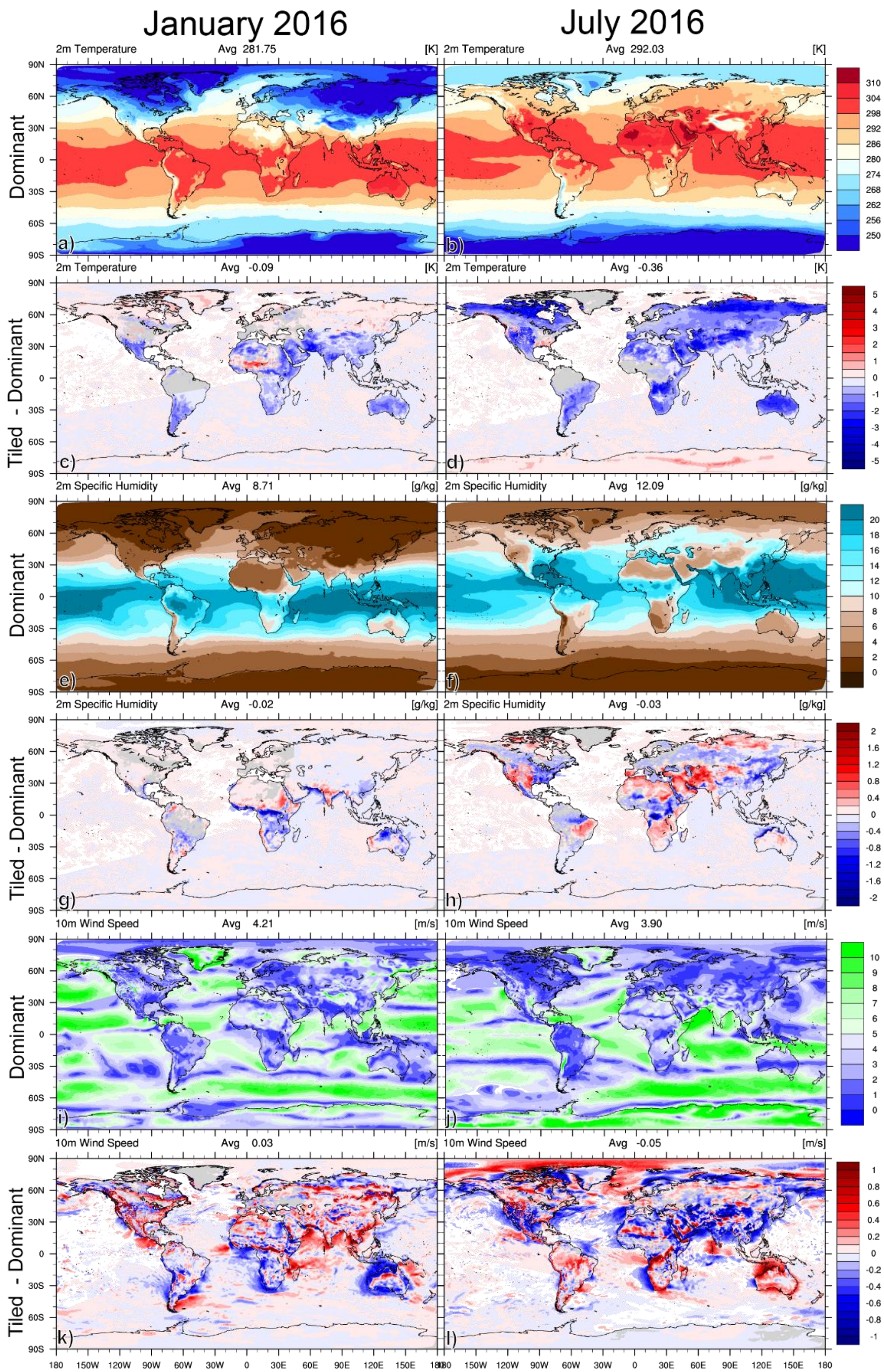

Figure 6. Average January and July 2016 dominant and difference plots (tiled – dominant) for the diagnostic variables a)-d) T2, e)-h) Q2, and i)-l) WSPD10 on the 92-25 km resolution mesh.

The tiled method results in global average cooling in both January (~ -0.1 K) and July 2016 (-0.4 K), which is due to widespread decreases in net SWDOWN, total net radiation, G (i.e., less heat flux into the ground), and the resulting available energy and partitioning (Supporting Figures S2-S5). The global increases in LH_flx and widespread decreases in SH_flx that result in widespread increases in the EF (Evaporative Fraction; See Section 1 for explanation), especially in July, results in a feedback that increases the low cloud water mixing ratio (especially in the Northern Hemisphere), decreases the net SW radiation at the surface, and decreases the overall net radiation (Figures S2-S5). Clearly the tiled method results in widespread global increases in the EF and decreases in T2, which may mitigate the systematic warm bias found in NWP models (Ma et al., 2014; Steiner et al., 2018 and references found within).

There is also a qualitative agreement for areas that are typical of higher (lower) temperatures (Figures 6a-b) with areas of decreased (increased) temperature due to tiled LCC (Figures 6c-d). The regions of lower (higher) humidity (Figures 6e-f) also agree with regions of increased (decreased) humidity (Figures 6g-h) due to tiling. The opposing directions of change in T2 and QSFC, particularly for the U.S. in July (see dipoles of change in the west and east U.S.), further indicates that the impacts of the tiled method are a result of changes in the surface energy balance and a shift in the partitioning of the SH_flx and LH_flx, which is due to the incorporation of appreciable fractions of various LU types in the mesh cells (Figures S2-S5). There are spatially variable impacts on WSPD10 with both increases and decreases (Figure 6i-l), but the impact of the tiled LCC is largest in July, and also leads to non-linear interactions in the northern high latitudes.

The impacts of the tiled method on EF also has feedbacks to the topmost soil temperature (TSLB) and moisture (SMOIS), as well as the planetary boundary layer height (PBLH) (Figure S6). In January, the TSLB increases in the high Northern latitudes and decreases in the low Northern latitudes and Southern Hemisphere. The increases (decreases) in TSLB qualitatively agree with decreases (increases) in SMOIS due to the effects of EF changes and cloud feedbacks on radiation. In July, the effects are similar but exacerbated, where there are widespread decreases in TSLB and increases in SMOIS, respectively, which is most prominent in the Northern Hemisphere mid- to high latitude regions where there are large increases in low cloud fraction. As expected, the increases (decreases) in PBLH are spatially well correlated with the regions of increases (decreases) in T2.

The spatial differences in tiled and diagnostic variables in January and July 2016 (Figures 4-6) are further elucidated when comparing the diurnal patterns of G, LH, SH, QSFC, and TSK for the dominant and 2nd ranked LU category, most notably in July (Figure 7).

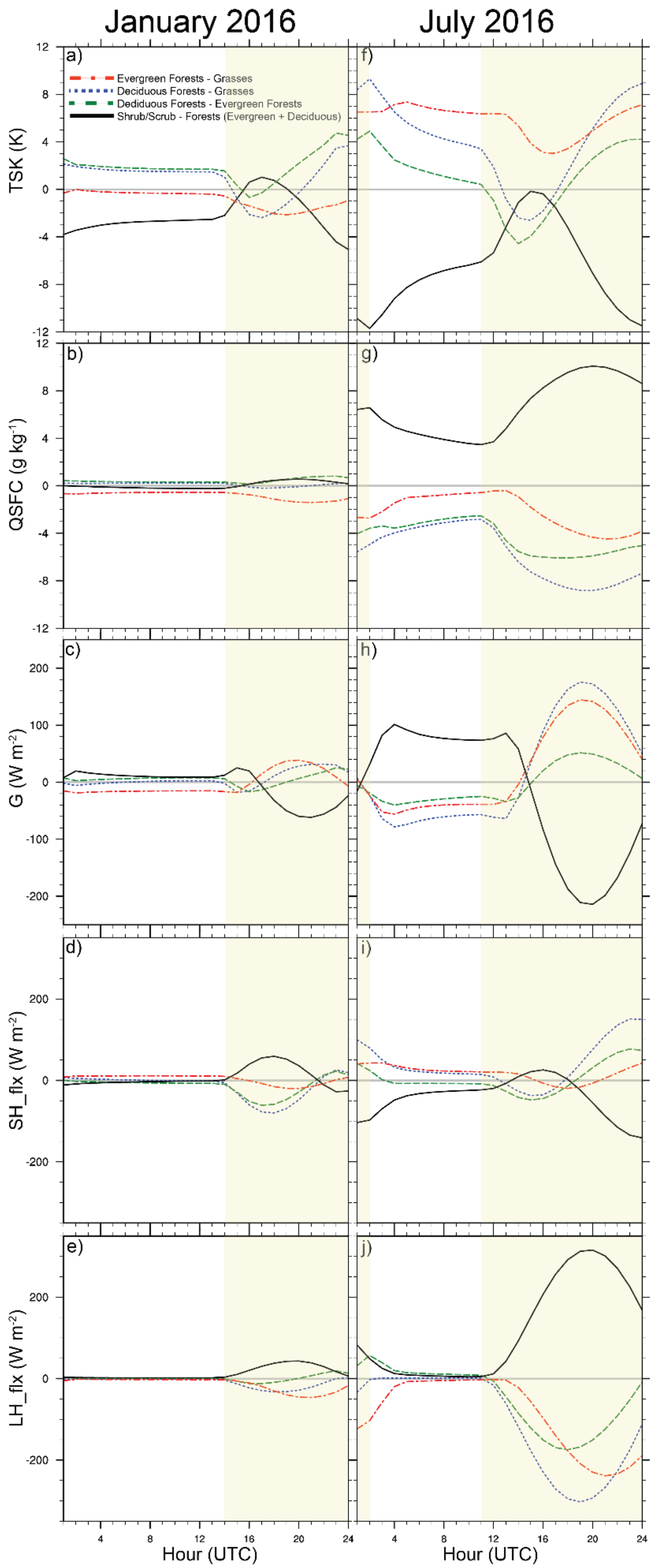

Figure 7. Diurnal analysis of the differences in dominant – 2nd ranked LU cateogory for TSK, QSFC, G, SH, and LH in a)-e) January and f)-j) July 2016. Analysis has been averaged over all CONUS grid cells. Approximate daytime hours for CONUS are shaded in light yellow.

In much of the central and western U.S. the widespread shrubs/grasses LU dominate the landscape (Figure 1), where including appreciable fractions of evergreen and decidous forest in the tiled approach leads to a net increase in heat flux into the ground (ΔG > 0) at the expense of sensible heat flux (ΔSH < 0), which results in cooler surface temperatures (ΔTSK < 0) at night in July (black line; Figure 7f-j). During the daytime transition period, the ΔG, ΔSH, and change in latent heat flux (ΔLH) approach zero, and there is a minimum in ΔTSK due to the tiled effects. Later in the daytime hours in July, however, the presence of more evergreen and deciduous forest result in a net loss of ground heat flux (ΔG < 0) which enhances latent heat flux to the atmosphere (ΔLH>0), where energy partitioning also requires that ΔSH<0 and consequently cooler surface temperatures, ΔTSK < 0. There is also a net increase in specific humidity (ΔQSFC>0) during both night and day in July due to the presence of more forest canopy and enhanced evapotranspiration (black line; Figure 7f-j). The opposite is true when including tiled fractions of shrubs/grasses LU types in either the dominant evergreen or deciduous forest regions, which are found mainly in the eastern U.S, and leads to predominantly drier (ΔQSFC<0) and warmer surface conditions (ΔTSK > 0) (red and blue lines; Figure 7f-j). A similar drier and warmer pattern is also true when including tiled fractions of evergreens LU types in cells that are dominated by decidous forest, as evergreens typically have less daytime transpiration (ΔLH<0) compared to deciduous trees in July (green lines; Figure 7f-j). In January, the diurnal patterns of G, LH, SH, QSFC, and TSK in January are similar to July, but have smaller amplitudes due to smaller net radiation energy for the U.S. winter, and consequently smaller magnitudes for the ΔG, ΔLH, and ΔSH partitioning (Figures 7a-7e).

3.2 Model evaluations of the MPAS-A dominant and tiled LCC approach

The tiled approach results in widespread reductions in MB for T2, Q2, and WSPD10 across the U.S. for a 92-25 km mesh during January and July 2016 (Figure 8). The largest, and most prolific reductions in MB are found in the western U.S. in July, where there are large decreases in T2 and increases in Q2 (Figures 8c-d and 8g-h). There are some smaller areas of increased MB for T2 and Q2, most notably in the southeast U.S. for July where increased temperatures exacerbate the simulated warm bias for T2, and in parts of the Central U.S. where decreases in predicted mixing ratio exacerbates the model dry bias for Q2. While more variable in nature, there are predominantly decreased MB for WSPD10 across the U.S. There are also widespread decreases in the RMSE for the tiled approach for T2, Q2, and WSPD10 (Supporting Figure S7).

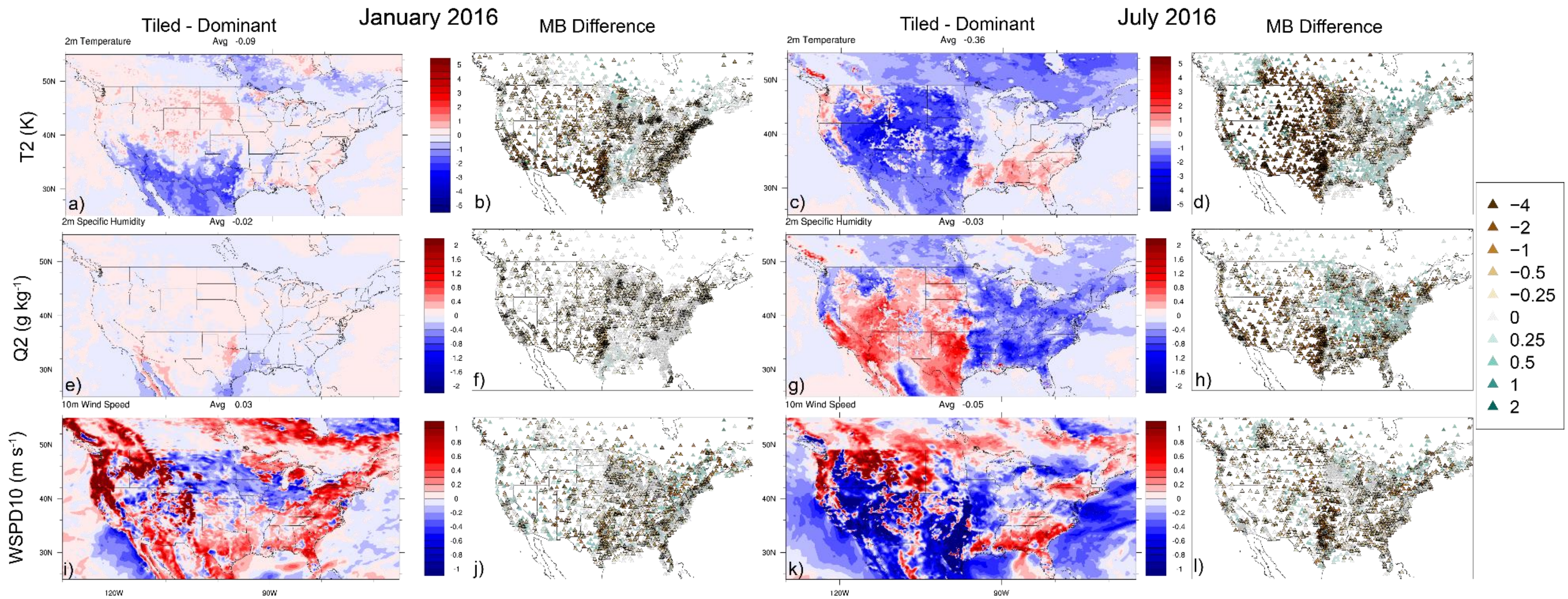

Figure 8. Average January (left) and July 2016 (right) absolute and MB difference (|tiled MB| – |dominant LCC MB|) compared against available MADIS-METAR stations for a)-d) T2, e)-h) Q2, and i)-l) WSPD10 on the 92-25 km resolution mesh.

The results from the 92-25 and 46-12 km meshes show a reduction in diurnal MB and RMSE for T2, Q2, and WSPD10 in the western U.S. during July, and there is preliminary indication of decreasing model sensitivity to the mesh resolution for T2 when using the tiled approach (i.e., MB red lines closer than blue lines) (Figures 9a-9b); however, testing of more resolutions are necessary for a full investigation of grid sensitivity. The impacts of the tiled approach are less for January in the eastern U.S., with some model degradation for similar reasons as discussed previously. The average CONUS and global statistical summaries (i.e., R, MB, RMSE, and IOA) are found in Supporting Tables S1 and S2. Overall, the largest model performance change in CONUS is for T2, where the average MB is reduced by a factor of ~ 4 due to the tiled approach. There is also lower MB for the WSPD10 in the western U.S. for July; however, there are increases in MB and RMSE for Q2 and WSPD10 in the eastern U.S. This dipole in model performance change apparent across CONUS is consistent with the strong east-west vegetation and moisture gradient and its interaction with the tiled compared to dominant LCC approaches.

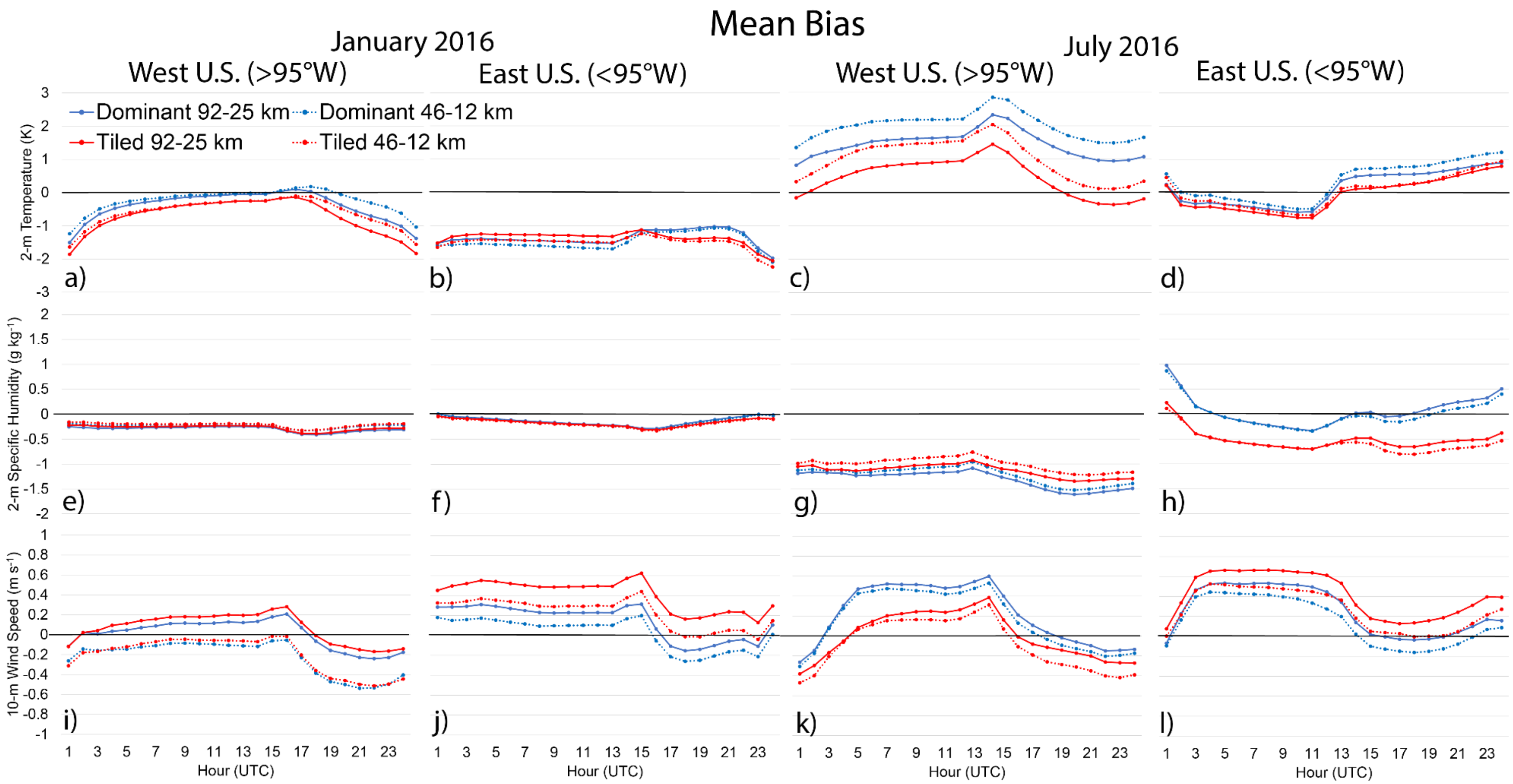

Figure 9a. Diurnal MB comparisons for a)-d) T2, e)-h) Q2, and i)-l) WSPD10 against MADIS-METAR for 92-25 and 46-12 km over eastern and western CONUS.

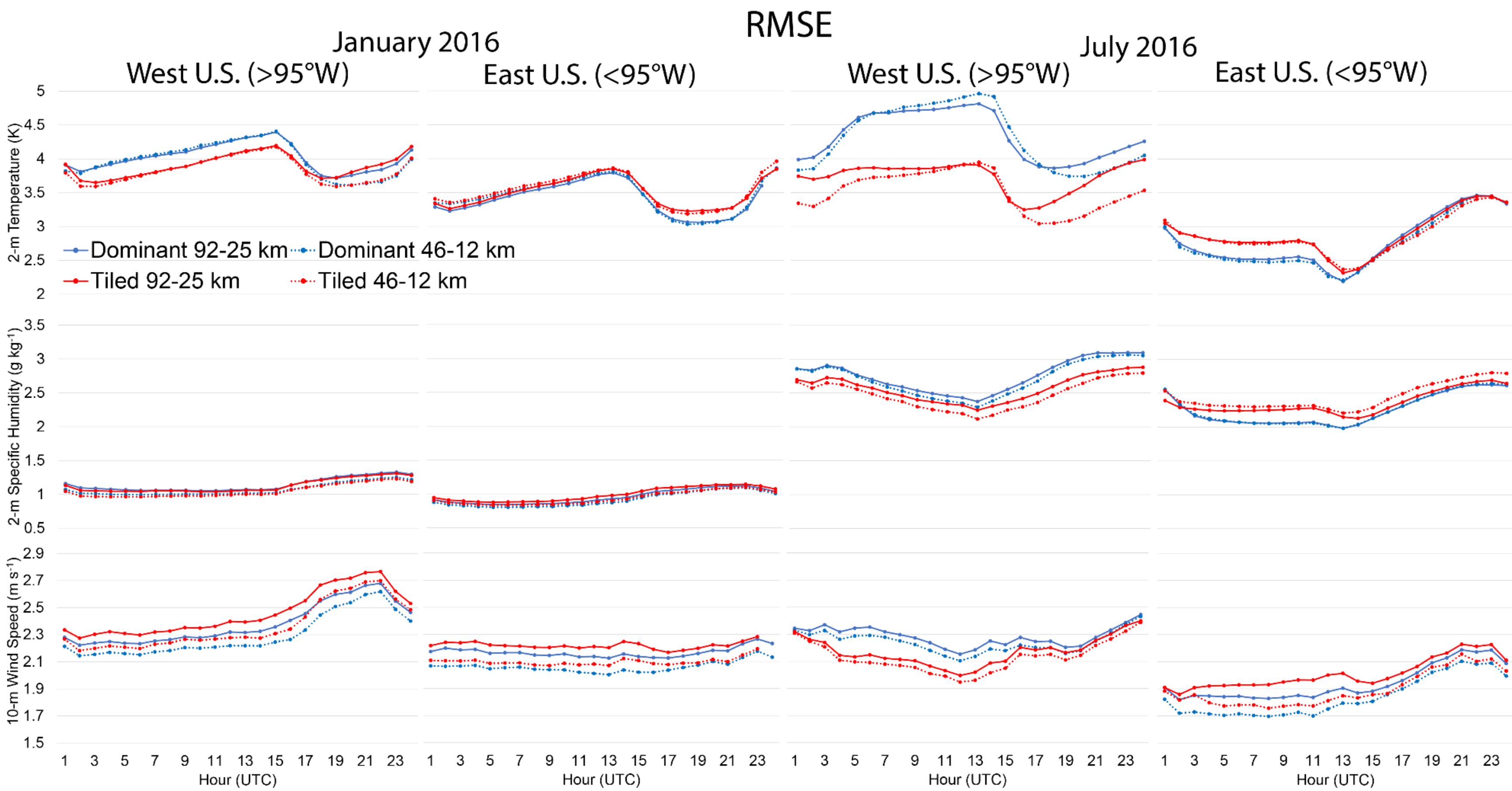

Figure 9b. Same as in Figure 9a, but for RMSE.

The effects of the tiled LCC approach on the partitioning of SH_flx and LH_flx and feedbacks to cloud formation also has implications for the total incoming SWDOWN (Figure 10).

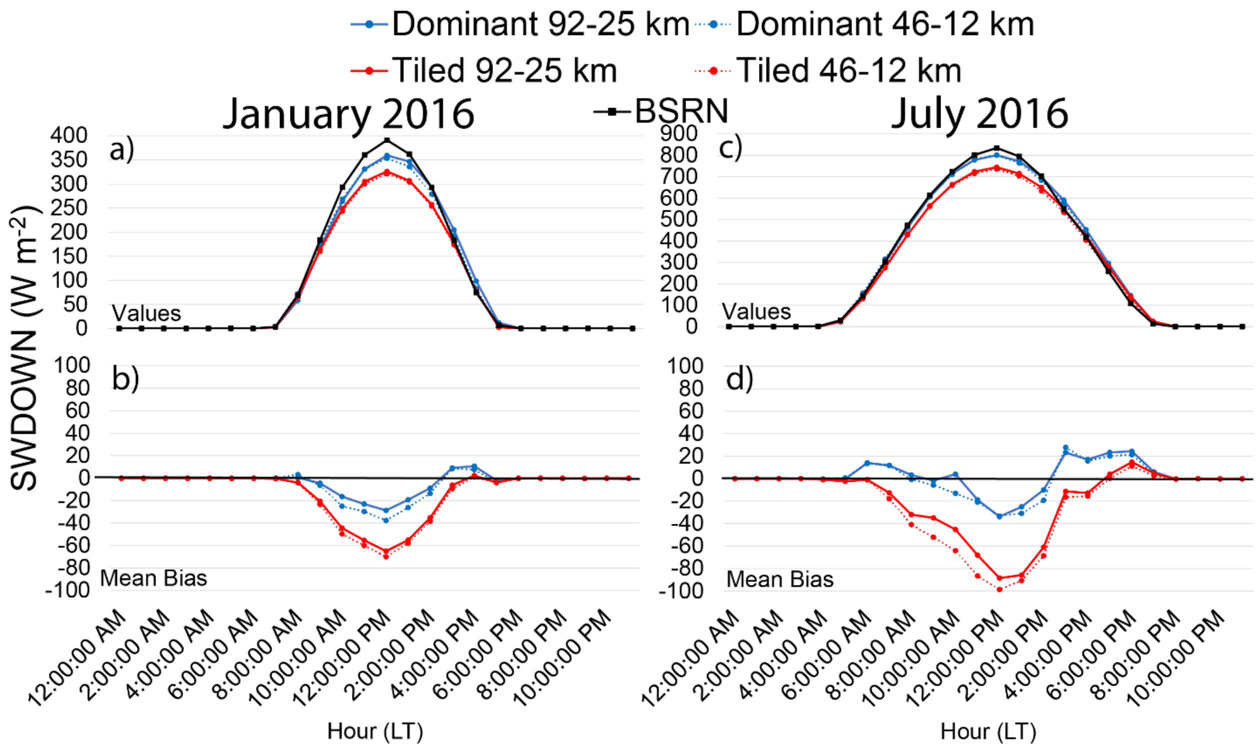

Figure 10. Average diurnal time series of SWDOWN and bias comparisons against BSRN for 10 CONUS sites for both 92-25 and 46-12 km meshes.

For an average of 10 BSRN sites across CONUS (Supporting Figure S8 contains a map of the U.S. sites), the tiled approach leads to an overall reduction in total SWDOWN during the local peak time, which leads to an overall increase in MB (and RMSE; see Supporting Figure S9) compared to the dominant LCC approach. This effect is more prominent during summer in July due to appreciable forest LU fractions included in the dominant shrublands/grasslands across the western U.S. (Figure 3h), and the resulting increase in EF (Figure S5), Q2 (Figure 6h), and low to high clouds that scatter incoming shortwave radiation. A spatial evaluation of SWDOWN against the global BSRN observation sites also shows increases in MB and RSME in the early to late afternoon hours due to the tiled approach, particularly in July 2016 for BSRN sites in the Northern Hemisphere (Supporting Figures S10-S11).

Incorporating more detailed and realistic LCC in MPAS-A leads to widespread model performance improvements (decreased MB and RMSE) for T2 and Q2, particularly in the western U.S., but a degradation (increased MB and RMSE) in the evaluation of SWDOWN driven by cloud-radiative feedback effects, both in the U.S. and globally. This result is the impact of a relatively "tuned" model performance towards more accurate predictions of near-surface temperature and moisture in MPAS-A (and other NWP models), at the expense of degrading performance (and more unknown) cloud-radiative feedback processes that affect the surface radiative balance (Ma et al., 2014).

The impact of the tiled approach on total precipitation over the U.S. is more scattered compared to PRISM observations, with both increases and decreases in MB compared to the dominant approach (Figure 11; Supporting Figure S12 shows the gridded 46-12 km PRISM data for comparison). For an average CONUS, however, there is a slight reduction in MB for precipitation due to the L13-tiled LCC, moreso for the 46-12 km compared to the 92-25 km mesh (Figures 11e-f). This is a result of reduced forest cover and slight decreases in EF in this region for the tiled approach, which deacreases precipitation and offsets the typical MPAS-A (and other NWP models) overprediction in eastern U.S. rainfall in the summer.

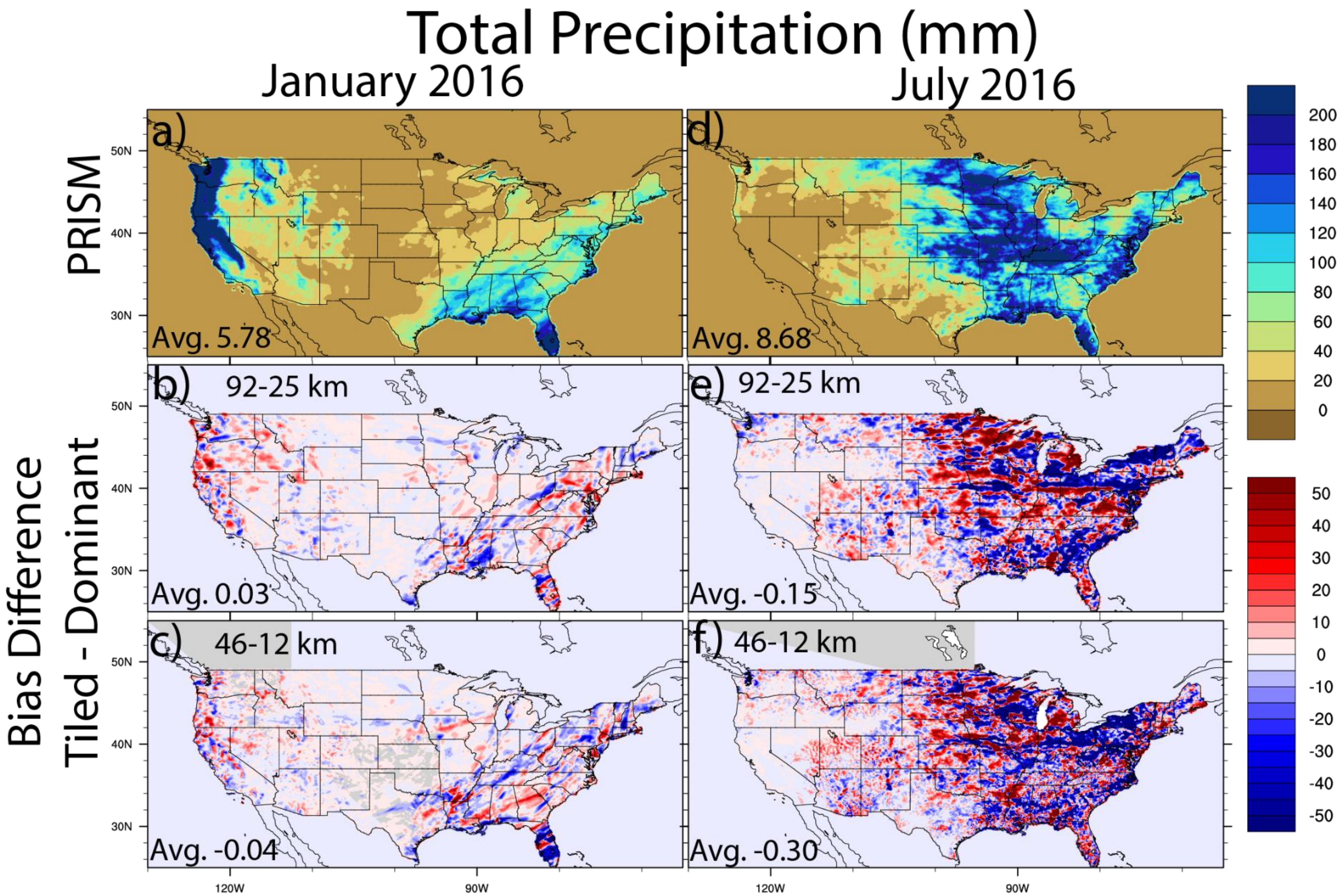

440

441 **Figure 11.** Total January and July 2016 PRISM precipitation observations gridded to the 92-25 km mesh (top) and the spatial bias
442 difference (|MB tiled| - |MB dominant|) for the 92-25 (middle) and 46-12 km meshes (bottom).

The impacts of the tiled approach extend above the surface as well, and there are increases in the IOA for the temperature, relative humidity, and wind speed profiles compared to RAOB sites across CONUS (Figure 12). The tiled approach shows increases in IOA for temperature up to about 500-600 hPa model heights for all the RAOB sites shown except in the northwest (Boise, Idaho; KBOI) and southwest U.S. (Salt Lake City, UT; KSLC). The relative humidity also shows increased IOA across an increased depth of the atmosphere (up to 200 hPa) for the central (Lincoln, IL; KILX) and northeast U.S. (Pittsburgh, PA; KPIT) compared to the dominant approach. There are slight decreases in IOA for the tiled approach in the lower atmosphere (> 800 hPa) in the upper midwest (Detroit, MI; KDTX) and western U.S. (Oakland, CA; KOAK), but overall there are larger increases in IOA compared to the decreases across the RAOB sites (i.e., generally improved model column performance). There are also larger increases in IOA for wind speed compared to the decreases for the tiled approach, where in some cases these increases are across a significant depth of the model column, e.g., in the south (Amarillo, TX; KAMA) and northeast U.S. (KPIT).

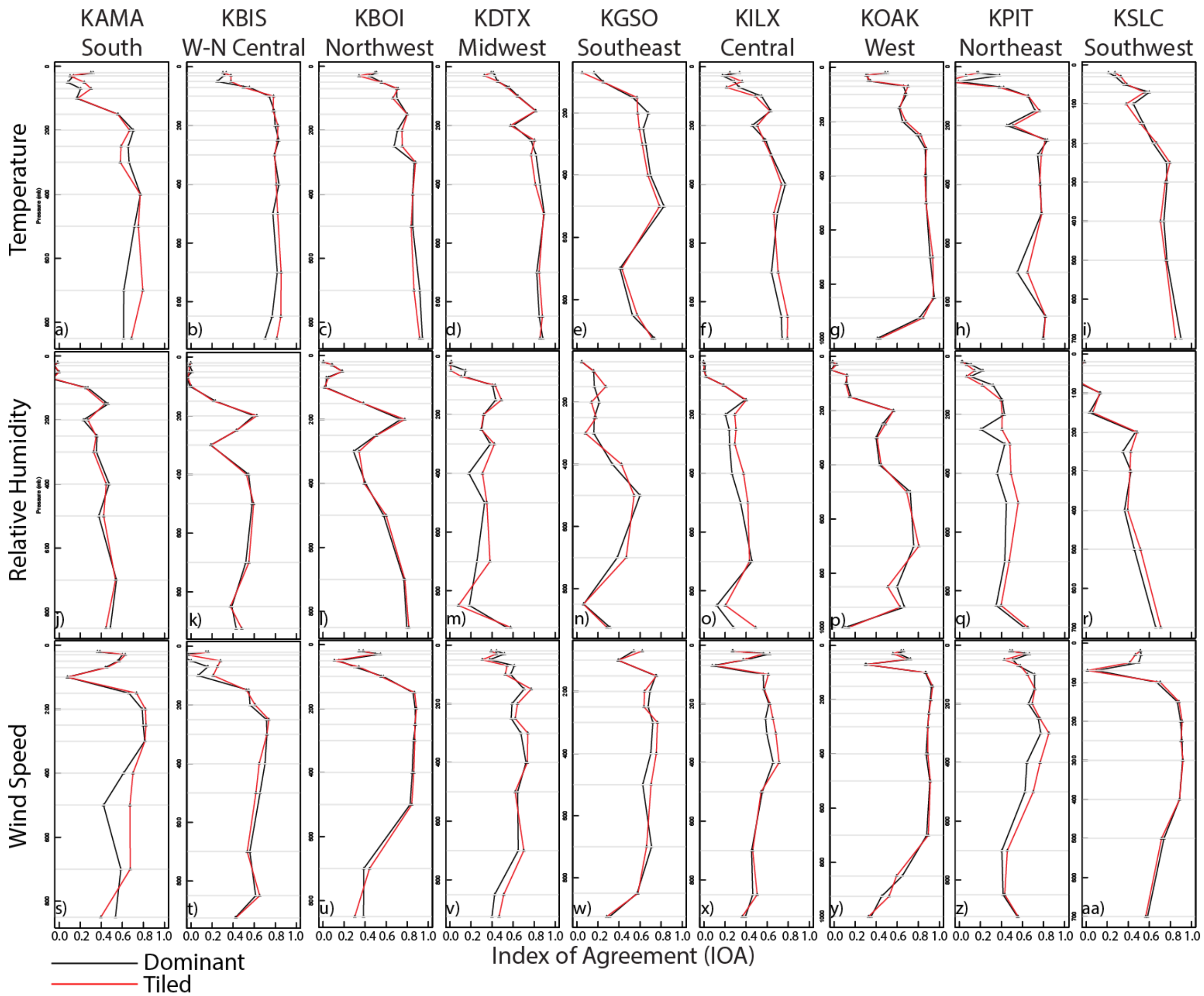

Figure 12. Vertical profiles of IOA compared against select RAOB sites across CONUS for temperature (top), relative humidity (middle), and wind speed (bottom) for the dominant (black) and tiled (red) approach for the 92-25 km mesh.

4. Summary and Implications

In this work a tiled approach to land cover characterization (LCC) in the Noah land surface model, following Li et al. (2013), is implemented in the Model for Prediction Across Scales – Atmosphere (MPAS-A), version 6.0, and was tested for January and July 2016 on both the 92-25 and 46-12 km refining meshes (focused on the conterminous U.S.; CONUS). Compared to the dominant LCC approach, the tiled LCC leads to significant impacts on global soil conditions, surface fluxes, near-surface and column meteorological variables, and cloud-radiative feedbacks. Specifically, the tiled LCC leads to both moderate warming and cooling in the Northern and Southern Hemisphere in January, respectively, with more dramatic, globally widespread cooling in July. For CONUS, there is a strong dichotomy of cooler and moister conditions in the west, and warmer and drier conditions in the east due to the tiled LCC. Such temperature and moisture changes are a result of shifts in tiled evergreen and deciduous forests, grasslands/shrublands, and urban land use in the eastern and western U.S. compared to the dominant approach, which alter the overall cloud-radiative balance, available energy, and diurnal partitioning between the ground, sensible, and latent heat fluxes. These changes in turn effect the development of near-surface wind flow, boundary layer heights, cloud formation processes, and resulting cloud-radiative feedbacks.

The tiled LCC has a strong impact on model performance, where there are significant reductions in both mean bias and root mean square error in CONUS for 2-m temperature, 2-m specific humidity, and 10-m wind speed. There is indication that the tiled LCC also reduces the sensitivity of predicted 2-m temperature to the finer 46-12 km mesh resolution in the eastern U.S. There are increases in model bias and error for incoming solar radiation, however, and the impacts on precipitation are more variable. There is an average decrease in mean bias for precipitation over the CONUS. The effect of the tiled LCC is felt through significant depths of the atmospheric column, and there is improved agreement of temperature, relative humidity, and wind speed with observations for many radiosonde observations across CONUS.

An important implication of this work is the effect of the tiled LCC on the evaporative fraction, cloud-radiative feedbacks, and the overall reduction in global temperatures in July (Northern Hemisphere summer). As demonstrated by the improved model performance for 2-meter temperature in CONUS, use of a tiled LCC could potentially help mitigate the systematic, global summertime warm biases that are apparent in most numerical weather prediction (NWP) models. The improved near-surface meteorology, but degraded performance in incoming solar radiation due to the more detailed tiled LCC further demonstrates that NWP models such as MPAS-A have experienced prolonged deficiencies in the LCC representation and processes, while being preferentially "tuned" to improve the above ground meteorological predictions despite unresolved cloud-feedbacks. The need for more iterative model developments with respect to LCC methodologies in LSMs and the impacts on soil/surface, meteorological, and cloud-feedbacks in NWP models cannot be overstated. While further testing is needed (e.g., a multi-year evaluation), it is further recommended that computationally efficient subgrid LCC schemes be continually developed and integrated in the LSMs coupled to global weather forecast models.

Acknowledgments

This research was performed while Patrick Campbell held a National Research Council Research Associateship Award at the U.S. Environmental Protection Agency. We thank Kiran Alapaty and Russell Bullock Jr. (U.S. EPA) and Fantine Ngan (NOAA/ARL) for providing valuable comments on a draft of this manuscript. We further acknowledge the MADIS-METAR, WRMC-BSRN, OSU-PRISM, and ESRL-RAOB observational networks for their data records. The modified MPAS-A version 6.0 source code with the tiled Noah LCC option is available on the corresponding author's GitHub page at https://github.com/drnimbusrain/MPAS-Release/tree/physics/noah_mosaic_updates.

Disclaimer

The scientific results and conclusions, as well as any views or opinions expressed herein, are those of the author(s) and do not necessarily reflect the views of U.S. EPA, NOAA, or the Department of Commerce.

References

Avissar, R. (1991), A statistical-dynamic approach to parameterize subgridscale land-surface heterogeneity in climate models, *Surv. Geophys*., 12(1–3), 155–178, https://doi.org/10.1007/Bf01903417.

Avissar, R., and R. A. Pielke (1989), A parameterization of heterogeneous land surfaces for atmospheric numerical-models and its impact on regional meteorology, *Mon. Weather Rev*., 117(10), 2113–2136, doi:10.1175/1520-0493(1989)117<2113:Apohls>2.0.Co;2.

Campbell, P. C., Bash, J. O., & Spero, T. L. (2019). Updates to the Noah land surface model in WRF-CMAQ to improve simulated meteorology, air quality, and deposition. *Journal of Advances in Modeling Earth Systems*, 11. https://doi.org/10.1002/2018MS001422

Driemel, A., Augustine, J., Behrens, K., Colle, S., Cox, C., Cuevas-Agulló, et al. (2018). Baseline Surface Radiation Network (BSRN): structure and data description (1992–2017). *Earth Syst. Sci. Data*, 10, 1491-1501. https://doi.org/10.5194/essd-10-1491-2018

Chen, F., & Dudhia, J. (2001). Coupling an advanced land surface-hydrology model with the Penn State-NCAR MM5 modeling system. Part I: Model implementation and sensitivity. *Mon. Wea. Rev.*, 129, 569-585. https://doi.org/10.1175/1520-0493(2001)129<0569:CAALSH>2.0.CO;2

Chen, F., Mitchell, K., Schaake, J., Xue, Y., Pan, H., Koren, V., et al. (1996). Modeling of land-surface evaporation by four schemes and comparison with FIFE observations. *J. Geophys. Res.*, 101, 7251-7268. https://doi.org/10.1029/95JD02165

Chen, F., Janjic, Z., & Mitchell, K. E. (1997). Impact of atmospheric surface-layer parameterizations in the new land-surface scheme of the NCEP mesoscale Eta model. *Bound. Layer Meteorol*. 85, 391–421. https://doi.org/10.1023/A:1000531001463

Chen, F., Manning, K.W., LeMone, M.A., Trier, S.B., Alfieri, J.G., Roberts, R., et al. (2007). Description and evaluation of the characteristics of the NCAR high-resolution land data assimilation system*. J. Appl. Meteorol. Climatol*., 46, 694–713. https://doi.org/10.1175/JAM2463.1

Ek, M. B., Mitchell, K. E., Lin, Y., Rogers, E., Grunmann, P., Koren, V., et al. (2003). Implementation of Noah land surface model advances in the National Centers for Environmental Prediction operational mesoscale Eta model. *J. Geophys. Res.*, 108, D22, https://doi.org/10.1029/2002JD003296

Emery, C., Zhen Liu, Armistead G. Russell, M. Talat Odman, Greg Yarwood & Naresh Kumar (2017) Recommendations on statistics and benchmarks to assess photochemical model performance, *Journal of the Air & Waste Management Association*, 67:5, 582-598, DOI: 10.1080/10962247.2016.1265027

Entekhabi, D., and P. S. Eagleson (1989), Land surface hydrology parameterization for atmospheric general circulation models including subgrid scale spatial variability, *J. Clim.*, 2(8), 816–831, https://doi.org/10.1175/1520-0442 (1989)002<0816:Lshpfa>2.0.Co;2

Famiglietti, J. S., and E. F. Wood (1991), Evapotranspiration and runoff from large land areas: Land surface hydrology for atmospheric general circulation models, *Surv. Geophys.*, 12(1–3), 179–204, https://doi.org/10.1007/Bf01903418

Giorgi, F., and R. Avissar (1997), Representation of heterogeneity effects in earth system modeling: Experience from land surface modeling, *Rev. Geophys.*, 35(4), 413–437, doi:10.1029/97RG01754.

Gollvik, S., and S. Samuelsson, (2011). A tiled land-surface scheme for HIRLAM. Swedish Meteorological and Hydrological Institute. SE-601 76 Norrkoping, Sweden.

Hibbard, K.A., F.M. Hoffman, D. Huntzinger, and T.O. West, 2017: Changes in land cover and terrestrial biogeochemistry. In: Climate Science Special Report: Fourth National Climate Assessment, Volume I [Wuebbles, D.J., D.W. Fahey, K.A. Hibbard, D.J. Dokken, B.C. Stewart, and T.K. Maycock (eds.)]. U.S. Global Change Research Program, Washington, DC, USA, pp. 277-302, doi: 10.7930/J0416V6X.

Koster, R. D., and M. J. Suarez (1992b), A comparative analysis of two land surface heterogeneity representations, *J. Clim.*, 5(12), 1379–1390. https://doi.org/10.1175/1520-0442(1992)005<1379:Acaotl>2.0.Co;2.

Li, R. and Arora, V. K. (2012): Effect of mosaic representation of vegetation in land surface schemes on simulated energy and carbon balances, *Biogeosciences*, 9, 593–605. https://doi.org/10.5194/bg-9-593-2012.

Li, D., Bou-Zeid, E., Barlage, M., Chen, F., & Smith, J. A. (2013). Development and evaluation of a mosaic approach in the WRF-Noah framework. *J. Geophys. Res. Atmos.*, 118, 11,918–11,935. https://doi.org/10.1002/2013JD020657.

Li, H., Wolter, M., Wang, X., & Sodoudi, S. (2017). Impact of land cover data on the simulation of urban heat island for Berlin using WRF coupled with bulk approach of Noah-LSM. *Theoretical and Applied Climatology*, 134(1-2), 67–81. https://doi.org/10.1007/s00704-017-2253-z

Ma, H., S. Xie, S.A. Klein, K.D. Williams, J.S. Boyle, S. Bony, H. Douville, S. Fermepin, B. Medeiros, S. Tyteca, M. Watanabe, and D. Williamson, 2014: On the Correspondence between Mean Forecast Errors and Climate Errors in CMIP5 Models. *J. Climate*, **27**, 1781–1798, https://doi.org/10.1175/JCLI-D-13-00474.1

Mallard, M. S., & Spero, T. L. (2018). Examining the effects of mosaic land cover on extreme events in historical downscaled WRF simulations. Poster Presented at the American Meteorological Society's Annual Meeting, Austin, TX.

Manrique-Suñén, A., A. Nordbo, G. Balsamo, A. Beljaars, and I. Mammarella (2013). Representing Land Surface Heterogeneity: Offline Analysis of the Tiling Method. *J. Hydrometeor.*, 14, 850–867, https://doi.org/10.1175/JHM-D-12-0108.1

Melton, J. R., & Arora, V. K. (2014). Subgrid scale representation of vegetation in global land surface schemes: implications for estimation of the terrestrial carbon sink. *Biogeosciences*, 11, 1021–1036. https://doi.org/10.5194/bg-11-1021-2014.

Mitchell, K.E., Lohmann, D., Houser, P.R., Wood, E.F., Schaake, J.C., Robock, A., et al. (2004). The multi-institution North American Land Data Assimilation System (NLDAS): utilizing multiple GCIP products and partners in a continental distributed hydrological modeling system. *J. Geophys. Res.*, 109, D07S90. https://doi.org/10.1029/2003JD003823

Morcrette, C. J., Van Weverberg, K.,Ma, H.-Y., Ahlgrimm, M., Bazile, E.,Berg, L. K., et al. (2018). Introduction to CAUSES: Description of weather and climate models and their near-surface temperature errors in 5day hindcasts near the Southern Great Plains. *Journal of Geophysical Research:Atmospheres*,123, 2655–2683. https://doi.org/10.1002/2017JD027199

Newman, A.J., M.P. Clark, A. Winstral, D. Marks, and M. Seyfried (2014): The Use of Similarity Concepts to Represent Subgrid Variability in Land Surface Models: Case Study in a Snowmelt-Dominated Watershed. *J. Hydrometeor*., 15, 1717–1738, https://doi.org/10.1175/JHM-D-13-038.1

Niu, G.-Y., Yang, Z.-L., Mitchell, K.E., Chen, F., Ek, M.B., Barlage, et al. (2011). The community Noah land surface model with multiparameterization options (Noah-MP): 1. Model description and evaluation with local-scale measurements. *J. Geophys. Res*. 116, D12109, https://doi.org/10.1029/2010JD015139

Pan, H.-L., & Mahrt, L. (1987). Interaction between soil hydrology and boundary layer development. *Boundary Layer Meteorol*., 38, 185– 202. https://doi.org/10.1007/BF00121563

Powers, J. G., Klemp, J. B., Skamarock, W. C., Davis, C. A., Dudhia, J., Gill, D. O., et al. (2017). The weather research and forecasting model: Overview, system efforts, and future directions. *Bulletin of the American Meteorological Society*, 98(8), 1717–1737. https://doi.org/10.1175/BAMS-D-15-00308.1

Samuelsson, S., Gollvik, S., & Ullerstig, A. (2006). The land surface scheme of the Rossby Centre Regional Atmospheric Climate Model (RCA3). *Meteorology* 122, SMHI, SE-601 76 Norrk¨oping, Sweden.

Skamarock, W. C., & Klemp, J. B. (2008). A time-split nonhydrostatic atmospheric model for weather research and forecasting applications. *Journal of Computational Physics*, 227(7), 3465–3485. https://doi.org/10.1016/j.jcp.2007.01.037

Skamarock, W.C., J.B. Klemp, M.G. Duda, L.D. Fowler, S. Park, and T.D. Ringler, 2012: A Multiscale Nonhydrostatic Atmospheric Model Using Centroidal Voronoi Tesselations and C-Grid Staggering. *Mon. Wea. Rev*., 140, 3090–3105, https://doi.org/10.1175/MWR-D-11-00215.1

Steiner, A. (2018), Diagnosing the warm bias in the central United States, Eos, 99, https://doi.org/10.1029/2018EO095669. Published on 23 April 2018.

Verseghy, D. L., McFarlane, N. A., and Lazare, M. (1993). CLASS – a Canadian land surface scheme for GCMs. 2. Vegetation model and coupled runs, *Int. J. Climatol*., 13, 347–370.

Yin, J., Zhan, X., Zheng, Y., Hain, C., Ek, M., Wen, J., et al. (2015). Improving Noah land surface model performance using near real time surface albedo and green vegetation fraction. *Agricultural and Forest Meteorology*, 218-219 https://doi.org/10.1016/j.agrformet.2015.12.001